



1 Characteristic features of latitudinal manifestations of the 23–24 2 April 2023 geomagnetic storm

3 Leonid F. Chernogor

4 Department of Space Radio Physics, V. N. Karazin Kharkiv National University, Kharkiv,
5 61022, Ukraine

6 Correspondence to: Leonid Chernogor (e-mail: Leonid.F.Chernogor@gmail.com)

7 Abstract. The paper examines, for the first time, the latitudinal dependence of variations in the geomagnetic field on
8 the surface of the Earth on the global scale during the severe two-step geomagnetic storm of 23–24 April 2023, a
9 major two-step storm in solar cycle 25. The data available at INTERMAGNET magnetometer network URL
10 (https://imag-data.bgs.ac.uk/GIN_VI/GINForms2) were chosen for two near-meridional chains of stations, one in
11 the western (eight stations) and the other in the eastern (ten stations) hemispheres, which were situated, for the first
12 time, in such a way that one of them was in the night hemisphere during both of the two steps of the geomagnetic
13 storm. One of the most interesting observations made show that during one step of the two-step storm part of the
14 near-Earth cross-tail current closed itself via the ionosphere, to which it was linked by the substorm current wedge,
15 and manifested itself in the magnetograms acquired at high and equatorial latitude stations on the night side of the
16 Earth. The two-step character of this storm has allowed us to suggest that the B_z interplanetary magnetic field
17 component threshold for the formation of the substorm current wedge lies in the $-(22-30)$ nT interval. Other
18 features of this two-step storm include the following. In the western hemisphere, the fluctuations of the geomagnetic
19 field strength on the days used as a quiet time reference period usually did not exceed a few tens of nanotesla (nT),
20 whereas in the course of the disturbed days, the variations in the geomagnetic field strength increased by a factor of
21 2 to 10 and reached a few hundred nT. In the eastern hemisphere during quiet times, the middle and low latitude
22 magnetometer stations generally recorded strength fluctuations smaller than 10–20 nT, while during the disturbed
23 period the fluctuations increased by a factor of 2–5 and greater, attaining $\pm(50-70)$ nT. The strength fluctuations
24 showed a considerable, up to 300–700 nT, increase at high latitudes. The northward component of the geomagnetic
25 field, X, exhibited the greatest perturbations at all latitudes in both hemispheres, as the level of strength fluctuations
26 decreased with decreasing latitude. The geomagnetic field strength fluctuations recorded at the magnetometer
27 stations nearly-equidistant from the equator were observed to be close in magnitude. Close in value also were the
28 strength fluctuations observed with the stations at close latitudes but in different hemispheres.

29 1 Introduction

30 Solar storms accompanied by solar flares, coronal mass ejections, the generation of shocks associated with coronal
31 mass ejections or fast solar wind streams, act to generate a complex set of processes in the solar-terrestrial system
32 comprised of the sun, interplanetary medium, magnetosphere, ionosphere, atmosphere, and solid earth to produce
33 geospace storms or to cause significant variations in space weather. A geospace storm includes synergetically



34 interacting storms in the magnetic field (geomagnetic storms), in the ionosphere (ionospheric storms), in
35 thermospheric neutral density variations, earlier termed the thermospheric storms (see, e.g., (Pröls and Roemer,
36 1987)), in the electric field in the magnetosphere, ionosphere, and atmosphere (electrical storms) (see, e.g.,
37 (Kleimenova et al., 2008; Chernogor and Domnin, 2014; Kleimenova et al., 2017; Chernogor, 2021a). Geospace
38 storms actually constitute the state of space weather. Space weather can have adverse effects on ground systems,
39 such as radars or power lines (effects involving magnetic-storm-induced geoelectrical currents), or space-, air-, and
40 ground-based communication links. The latter include errors in Global Positioning System and in VLF navigation
41 systems, loss of HF communications, disruption of UHF satellite links due to scintillations, etc. Disturbances appear
42 in all ranges of radio waves, from VLF to UHF. Thus, many of humankind's technological systems are susceptible
43 to failure or unreliable performance because of geospace storms, and therefore the study of the manifestations of
44 geospace storms in all geospheres and geophysical fields remains an important task.

45
46 The manifestations of geomagnetic storms have been studied better than those of the other kinds of storm. They are
47 dealt with in a large number of studies (see, e.g., (Gonzalez et al., 1994; Laštovička, 1996; Fuller-Rowell et al.,
48 1997; Buonsanto, 1999; Danilov and Laštovička, 2001; Chernogor et al., 2007; Chernogor, 2021b; Lin et al., 2022;
49 Al Shidi et al., 2022; Hsu and Pedatella, 2023)) and in books (Pröls, 1995; Daglis, 2001; Freeman, 2001; Song et
50 al., 2001; Carlowicz and Lopez, 2002; Bothmer and Daglis, 2006; Lilensten and Bornarel, 2006; Kamide and
51 Maltsev, 2007; Moldwin, 2008; Koskinen, 2011). The main concern was to study the most severe storms, since they
52 have the strongest impact on human well-being and the correct functioning of space-based and ground-based
53 systems and can affect human health (Daglis, 2001; Freeman, 2001; Song et al., 2001; Carlowicz and Lopez, 2002;
54 Moldwin, 2008).

55
56 Dozens of studies have been devoted to only one of many magnetic storms, a solar cycle 24 major storm, which
57 occurred in September 2017 (see, e.g., (Song et al., 2001; Qian et al., 2019; Chernogor and Shevelev, 2020;
58 Oikonomou et al., 2022; Fagundes et al., 2023)). Examples of other magnetic storms that occurred over 2016–2022
59 are described in (Chernogor, 2021a, 2021b; Chernogor et al., 2021; Katsko et al., 2021; Luo et al., 2021a, 2021b,
60 2022; Luo and Chernogor, 2022; Laskar et al., 2023). The statistical analysis of the geomagnetic storm effects has
61 been performed in (Chernogor, 2021b; Abe et al., 2023; De Abreu et al., 2023).

62
63 The study of geomagnetic storms remains one of the main problems in space physics. This occurs for a few reasons.
64 First, every magnetic storm has its own individual features, in addition to the general characteristics. Second, the
65 manifestation of magnetic storms is dependent on the solar storm parameters and features, the general state of space
66 weather, geographic coordinates, local time, and solar cycle phase. The purpose of this paper is to analyze
67 characteristic features of latitudinal manifestations of the 23–24 April 2023 geomagnetic storm, a major two-step
68 storm in solar cycle 25 to date. The main features of the coronal mass ejection that caused this two-step storm can be
69 summarized as follows (Ghag et al., 2024). First, the storm lacked sudden storm commencement. Instead, the
70 interplanetary magnetic field B_z component turned southward at 17:37 UTC on 23 April 2023 and remained negative



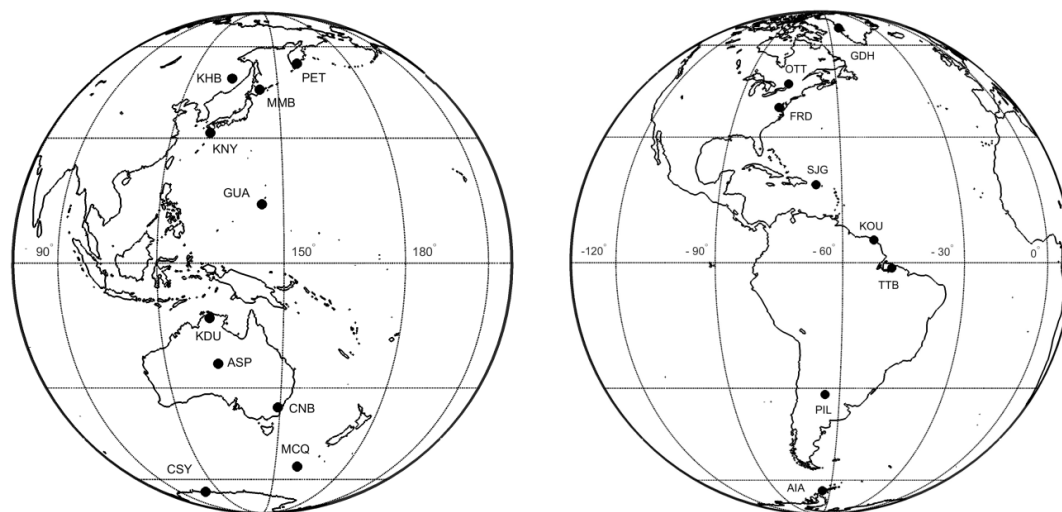
71 for about three hours, after which B_z was fluctuating during the sheat transit till almost 01:00 UTC on 24 April 2023
72 with $B_z \sim -22$ nT (<https://spaceweather.com/images2023/25apr23/cmeimpact.jpg>). This process was the likely cause
73 of the first step of the severe geomagnetic storm. Next, a magnetic cloud transit occurred, with $B_z \sim -30$ nT, which
74 was the cause of the second step of the storm under study. The two magnetometer chains employed in this study
75 were situated, for the first time, in such a way that one of them was in the night hemisphere of the Earth during both
76 of the two steps of the 23–24 April 2023 geomagnetic storm. The paper begins with a description of instrumentation
77 and the state of space weather. This information is followed by analysis of variations in the geomagnetic field under
78 disturbed and quiet time conditions. The paper ends with a discussion of the results obtained and conclusions drawn.

79 2 Instrumentation and techniques

80 The data available at INTERMAGNET magnetometer network URL ([https://imag-](https://imag-data.bgs.ac.uk/GIN_VI/GINForms2)
81 [data.bgs.ac.uk/GIN_VI/GINForms2](https://imag-data.bgs.ac.uk/GIN_VI/GINForms2); retrieved 22 November 2023) from two near-meridional chains of stations, one
82 in the western (eight stations) and the other in the eastern (ten stations) hemispheres, have been retrieved (Fig. 1).
83 The observatories in the western hemisphere are listed in Table 1 and those in the eastern hemisphere are presented
84 in Table 2. The magnetometers acquired measurements with 1-nanotesla (nT) strength resolution at one min
85 intervals. Analysis of temporal variations in the strength of the northward, X, eastward, Y, and vertical, Z,
86 components of the geomagnetic field over the period 20–26 April 2023 has been performed.

87

88 The data processing technique is as follows. First, the data on the absolute value of time variations are used to
89 calculate the diurnal trend. Then, the diurnal trend is subtracted from the primary time series resulting in the time
90 series of relative magnitudes. The relative magnitudes of variations in all components of the geomagnetic field are
91 subjected to further analysis.



92 **Figure 1: Map showing the recording stations.**

94 **Table 1** Observatories in the western hemisphere.



IAGA code, name, country	Geographic*		Corrected Geomagnetic*	
	Lat.	Long.	Lat.	Long.
GDH, Godhavn, Greenland	69.251°N	306.471°E	74.11°N	36.89°E
OTT, Ottawa, Canada	45.403°N	284.448°E	53.88°N	2.94°E
FRD, Fredericksburg, United States of America	38.205°N	282.627°E	47.13°N	359.97°E
SJG, San Juan, United States of America	18.111°N	293.85°E	25.23°N	12.27°E
KOU, Kourou, French Guiana**	5.209°N	307.267°E	13.99°N	20.49°E
TTB, Tatuoca, Brazil**	-1.201°N	311.494°E	7.37°N	24.38°E
PIL, Pilar, Argentina	-31.667°N	296.117°E	-21.13°N	5.43°E
AIA, Akademik Vernadsky, Antarctica	-65.246°N	295.743°E	-51.06°N	9.27°E

95 * The coordinates are retrieved from the list of geomagnetic observatories at
 96 https://isgi.unistra.fr/listobs_index.php?index=SSC.

97 ** The geomagnetic coordinates are not corrected.

98

99

Table 2 Observatories in the eastern hemisphere.

IAGA code, name, country	Geographic		Geomagnetic	
	Lat.	Long.	Lat.	Long.
PET, Paratunka (Petropavlovsk), Russian Federation	52.971°N	158.248°E	46.71°N	228.5°E
KHB, Khabarovsk, Russian Federation	47.61°N	134.69°E	41.65°N	208.57°E
MMB, Memambetsu, Japan	43.91°N	144.189°E	37.29°N	217.11°E
KNY, Kanoya, Japan	31.425°N	130.88°E	25.04°N	204.35°E
GUA, Guam, United States of America	13.59°N	144.87°E	6.28°N	217.04°E
KDU, Kakadu, Australia	-12.686°N	132.472°E	-21.46°N	204.44°E
ASP, Alice Springs, Australia	-23.76°N	133.885°E	-33.53°N	207.84°E
CNB, Canberra, Australia	-35.313°N	149.364°E	-44.98°N	227.56°E
MCQ, Australia	-54.5°N	158.935°E	-63.92°N	248.84°E
CSY, Casey Station, Australia	-66.282°N	110.528°E	-80.49°N	159.89°E

100 * The coordinates are retrieved from the list of geomagnetic observatories at

101 https://isgi.unistra.fr/listobs_index.php?index=SSC.

102 3 Space weather

103 The data involved in the analysis of space weather include the temporal variations of solar wind parameters
 104 (<https://omniweb.gsfc.nasa.gov/form/dx1.html>), the interplanetary magnetic field (IMF), the storm-time variation,
 105 D_{st} , and the three-hour planetary, K_p , indices (<https://wdc.kugi.kyoto-u.ac.jp/>), as well as calculated solar wind
 106 dynamic pressure and the Akasofu energy function, all of which are presented in Fig. 2.

107

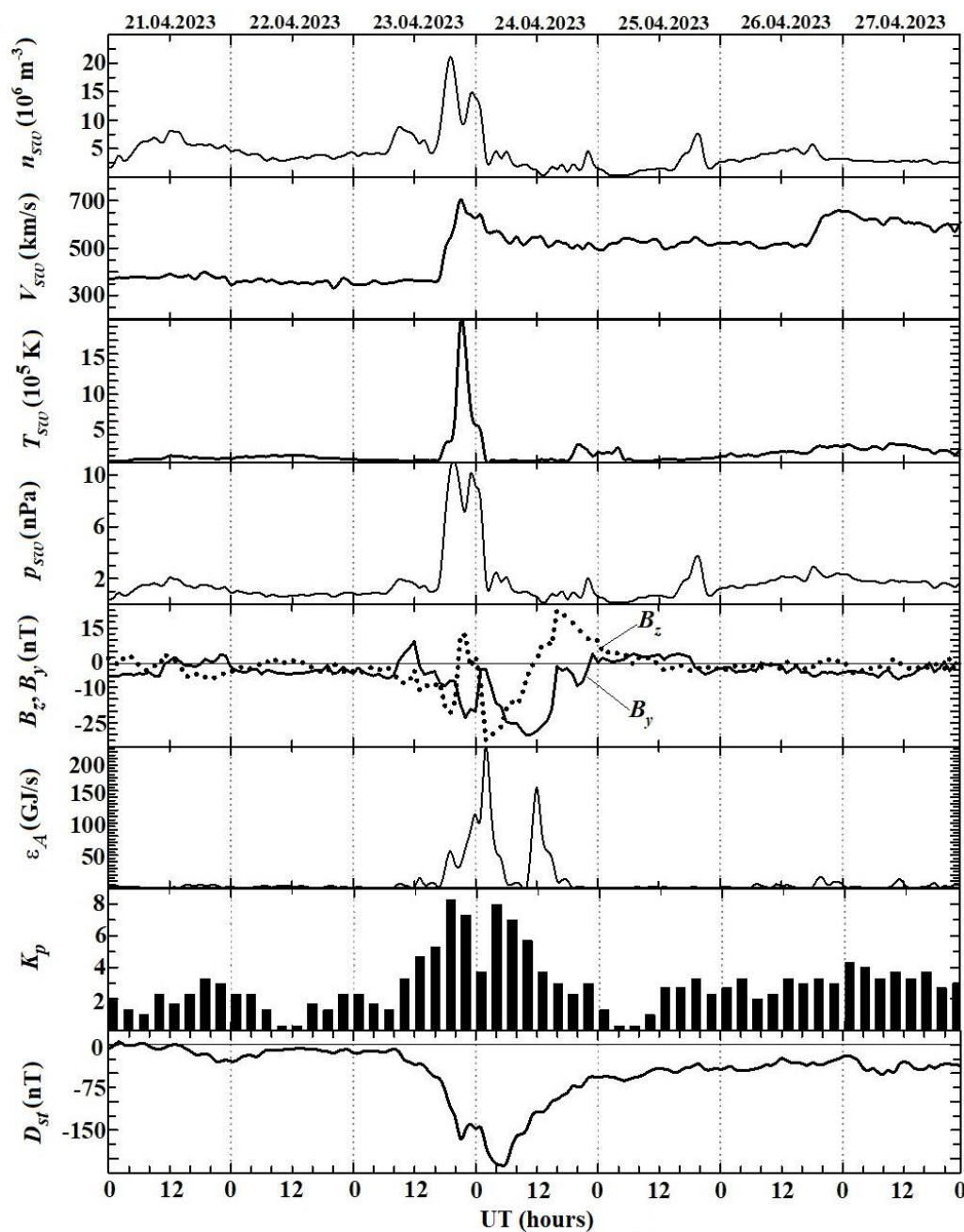
108 During the 23–24 April 2023 storm, the solar wind showed a peak in the proton density of $21.1 \times 10^6 \text{ m}^{-3}$ from a
 109 background of $(5-10) \times 10^6 \text{ m}^{-3}$, when the solar wind speed exhibited an enhancement to 706 km/s from a
 110 background of 350–400 km/s observed prior to the storm. These enhancements were accompanied by a rise in the
 111 dynamic pressure of 11 nPa from a background of 1–3 nPa, and by an increase in the temperature of $20.5 \times 10^5 \text{ K}$



112 from a background of $(1-2)\times 10^5$ K. Under quiet conditions, the strengths of the IMF B_y and B_z components usually
113 did not exceed ± 5 nT, whereas they significantly increased on 23 and 24 April 2023, with $B_{y\max} \approx 9.5$ nT, $B_{y\min} \approx -$
114 30.2 nT, $B_{z\max} \approx 10.5$ nT, and $B_{z\min} \approx -32.4$ nT. In the course of the magnetically quiet period, the Akasofu function
115 was smaller than 10 GJ/s, whereas two large peaks of up to 220 GJ/s and 160 GJ/s were observed to persist for 14 h
116 and 7 h, respectively, during 23 and 24 April 2023.

117

118 The magnitude of the background K_p index varied from 0 to 3, whereas it increased from 4 to 8.3 after 12:00 UT on
119 23 April 2023 and further decreased to 4. Yet another increase in the K_p index, up to 8, was observed between 03:00
120 UT and 06:00 UT on 24 April 2023. Before 08:00 UT on 23 April 2023, the magnitude of D_{st} varied from -30 nT to
121 5 nT. Over the interval 08:00–21:00 UT on 23 April 2023, its magnitude decreased from 10 nT to -170 nT. A new
122 decrease in D_{st} , from -150 nT to -212 nT, was observed during the interval 01:00 UT to 05:00–06:00 UT on 24
123 April 2023. After the latter, the D_{st} index increased from -212 nT to -25 nT. Thus, this storm is the first two-step
124 severe geomagnetic storm in solar cycle 25 caused by a coronal mass ejection that arrived at Earth at 19:26 UTC on
125 23 April 2023 (Ghag et al., 2024).



126
 127 **Figure 2:** UT variations in the solar wind parameters: measured proton number density, n_{sw} , temperature,
 128 T_{sw} , plasma flow speed, V_{sw} , calculated dynamic pressure, p_{sw} , measured B_z and B_y components of the
 129 interplanetary magnetic field; variations of the calculated magnitude of the energy, ϵ_A , deposited into the
 130 Earth's magnetosphere from the solar wind per unit time; K_p - and D_{st} indices for the period April 21 – 27,
 131 2023 (retrieved from <https://omniweb.gsfc.nasa.gov/form/dx1.html>;
 132 last access: 14 November 2023). Dates are indicated at the top of the figure.



133 **4 Analysis of magnetometer data**

134 **4.1 Western hemisphere**

135 *GDH Station*. From 00:00 UT to 10:00 UT over the geomagnetically quiet interval 20–22, 25, and 26 April 2023,
136 the strength of the northward component of the geomagnetic field, X , showed fluctuations within ± 50 nT (Fig. 3),
137 while between 10:00 UT and 18:00 UT the strength fluctuations increased to 60–145 nT with the energy spectrum
138 almost flat. On 23 April 2023, the variations in the X -component developed into non-monotonous and even quasi-
139 periodic changes between 10:00 UT and 24:00 UT, when the X -component strength varied from 120 nT to 180 nT.
140 Considerable disturbances, up to -550 nT, took place at around 11:15 UT on 24 April 2023, and only after 16:00 UT
141 on 24 April 2023 the level of fluctuations approached ± 50 nT. The recovery phase persisted for 25 and 26 April
142 2023.

143
144 Between 00:00 UT and 10:00 UT on 20–23 and 25, 26 April 2023, the variations in the eastward component of the
145 geomagnetic field, Y , were relatively insignificant, up to 50 nT, while between 10:00 UT and 18:00 UT, they were
146 observed to reach up to ± 100 nT. The variations in the Y -component showed non-monotonousness and, at times,
147 quasi-periodicity over a span of 14 hours from 10:00 UT to 24:00 UT on 23 April 2023, with a drop in the strength
148 down to -220 nT after 19:30 UT. From 11:00 UT to 12:00 UT on 24 April 2023, the strength varied from 340 nT to
149 -300 nT.

150
151 On 20–23 and 25, 26 April 2023, the variations in the vertical component of the geomagnetic field, Z , strength were
152 quite smooth, within ± 100 nT from 00:00 UT to 08:00 UT, while after 10:00 UT and towards the end of the day, the
153 variations enhanced, with peak-to-peak amplitude attaining 340 nT. Between 00:00 UT and 14:00 UT on 23 April
154 2023, the Z -component showed significant fluctuations in strength, with peak-to-peak amplitude of 150 nT and a
155 maximum of 100 nT. During the period 12:00 UT on 23 April 2023 to 14:00 UT on 24 April 2023, the strength
156 variations exhibited non-monotonousness and, at times, quasi-periodicity. At about 20:00 UT on 23 April 2023, the
157 strength reached -230 nT. After 09:00 UT on 24 April 2023, the strength varied from 380 nT to -430 nT, which was
158 recorded between about 11:00 UT and 12:00 UT.

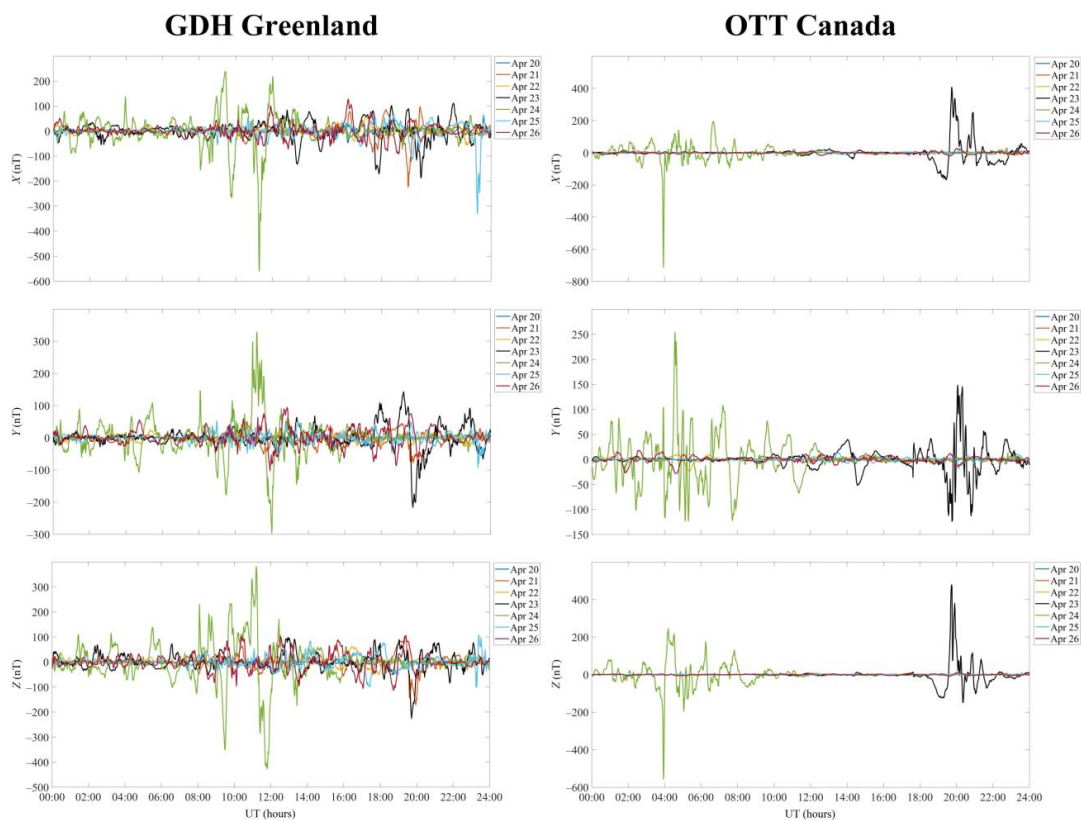


Figure 3: UT variations of the geomagnetic field at the GDH station (geographic coordinates 69.2520°N, 53.5330°W, geomagnetic coordinates 77.52°N, 32.69°E) and at the OTT station (geographic coordinates 45.4030°N, 75.552°W, geomagnetic coordinates 54.46°N, 3.51°W) over the period 20–26 April 2023.

159
160
161
162

163

164 *OTT Station.* On the days used as a quiet time reference period, the variations in the strength of the northward
165 component of the geomagnetic field, X , rarely exceeded ± 20 nT (Fig. 3). On 23 April 2023, sharp increases of up to
166 250–420 nT in the strength of the X -component were observed from 19:30 UT to 22:00 UT; and from 21:00 UT to
167 22:30 UT, the X -component strength decreased approximately to -100 nT. Between 03:00 UT and 09:30 UT on 24
168 April 2023, the magnetic field strength fluctuated mainly from -100 nT to 200 nT, and only at 03:55 UT, it briefly
169 dropped to -710 nT. Immediately after 14:00 UT on 24 April 2023, the variations in the X -component strength
170 became smaller than a few tens of nT.

171

172 Monotonous variations in the eastward component of the geomagnetic field, Y , strength did not exceed ± 30 nT
173 during geomagnetically quiet times, whereas over the period 10:00 UT on 23 April 2023 to 13:00 UT on 24 April
174 2023, the Y -component exhibited large fluctuations in strength, from -125 nT to 257 nT.

175

176 During magnetically quiet times, the vertical component of the geomagnetic field, Z , strength showed quite smooth
177 variations, the amplitude of which was smaller than a few tens of nT. During the period 19:00 UT on 23 April 2023
178 to 10:00 UT on 24 April 2023, the Z -component fluctuated wildly, first from -140 nT to 490 nT near 19:40 UT on
179 23 April 2023, then within ± 80 nT after 00:00 UT, and then it decreased to -560 nT at around 03:55 UT on 24 April
180 2023.

181

182 *FRD Station.* The variations in the northward component of the geomagnetic field, X , did not exceed 10–15 nT
183 during magnetically quiet times (Fig. 4), while between about 10:00 UT on 23 April 2023 and 12:00 UT on 24 April



184 2023, its variations showed non-monotonousness, and an increase in X -component strength that occurred over the
185 interval 19:45–23:35 UT. The X -component exhibited fluctuations within -52 – 67 nT on 24 April 2023, with a
186 minimum of -76 nT at about 04:10 UT; after about 12:00 UT, significant variations ceased.
187

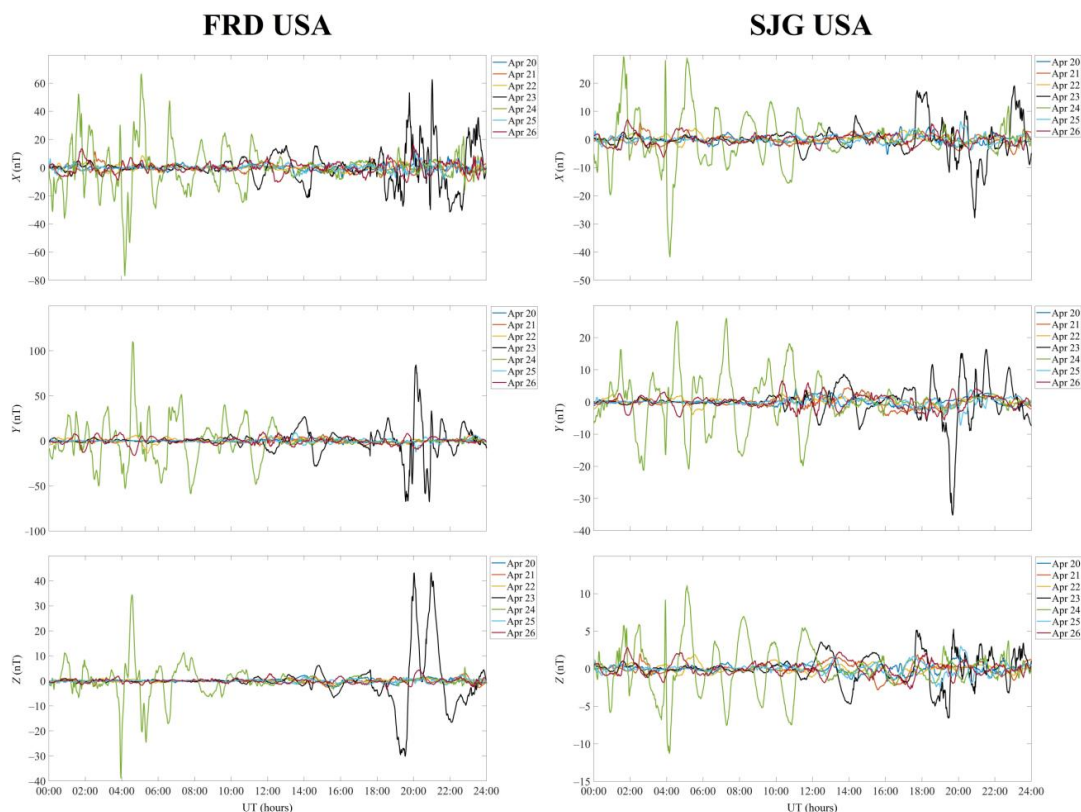
188 During magnetically quiet times, the variations in the eastward component of the geomagnetic field, Y , strength were
189 smaller than ± 20 nT, including the disturbance-daily variation. During a period from 10:00 UT on 23 April 2023 to
190 13:00 UT on 24 April 2023, the strength fluctuations were large, with a minimum of -70 nT that occurred between
191 19:30–21:00 UT on 23 April 2023. An increase in the strength within -60 – 115 nT was observed to occur between
192 02:00 UT and 12:00 UT on 24 April 2023.
193

194 Over a span of magnetically quiet times, the vertical component of the geomagnetic field, Z , strength, weakly
195 fluctuating, changed its magnitude by less than 5 nT. The noticeable variations in its magnitude began at around
196 14:00 UT on 23 April 2023 and ended at about 12:00 UT on 24 April 2023, with maximums of ~ 44 nT observed at
197 around 20:00 UT and 21:00 UT on 23 April 2023, and a minimum of -39 nT at about 04:00 UT on 24 April 2023.
198

199 *SJG Station*. During magnetically quiet times, the fluctuations in strength of the northward component of the
200 geomagnetic field, X , were smaller than ± 7 nT (Fig. 4). The noticeable variations in strength began at around 11:00
201 UT on 23 April 2023 and were over past 14:00 UT on 24 April 2023, with minimums of about -28 nT at
202 approximately 20:50 UT on 23 April 2023 and of about -42 nT at around 04:10 UT on 24 April 2023, and with
203 maximums of 30 nT at about 01:30 UT and 05:00 UT on 24 April 2023.
204

205 The eastward component of the geomagnetic field, Y , strength showed insignificant variations, ~ 7 nT, before 10:00
206 UT on 20–23 and 25, 26 April 2023, while between 10:00 UT on 23 April 2023 and 14:00 UT on 24 April 2023, the
207 Y -component strength exhibited non-monotonous and significant disturbances, with a minimum of about -35 nT at
208 19:40 UT on 23 April 2023 and a maximum of about 26 nT at 07:15 UT on 24 April 2023.
209

210 During magnetically quiet times, the vertical component of the geomagnetic field, Z , strength showed variations
211 smaller than ± 3 nT. The non-monotonous and significant fluctuations in the strength of this component were
212 observed to occur starting at 12:00 UT on 23 April 2023 and ending at 14:00 UT on 24 April 2023, with a minimum
213 of about -11.5 nT and a maximum of about 11.5 nT.



214
215
216
217

Figure 4: UT variations of the geomagnetic field at the FRD station (geographic coordinates 38.2100°N, 77.3670°W, geomagnetic coordinates 47.25°N, 5.47°W) and at the SJG station (geographic coordinates 18.1100°N, 66.1500°W, geomagnetic coordinates 27.20°N, 6.96°E) over the period 20–26 April 2023.

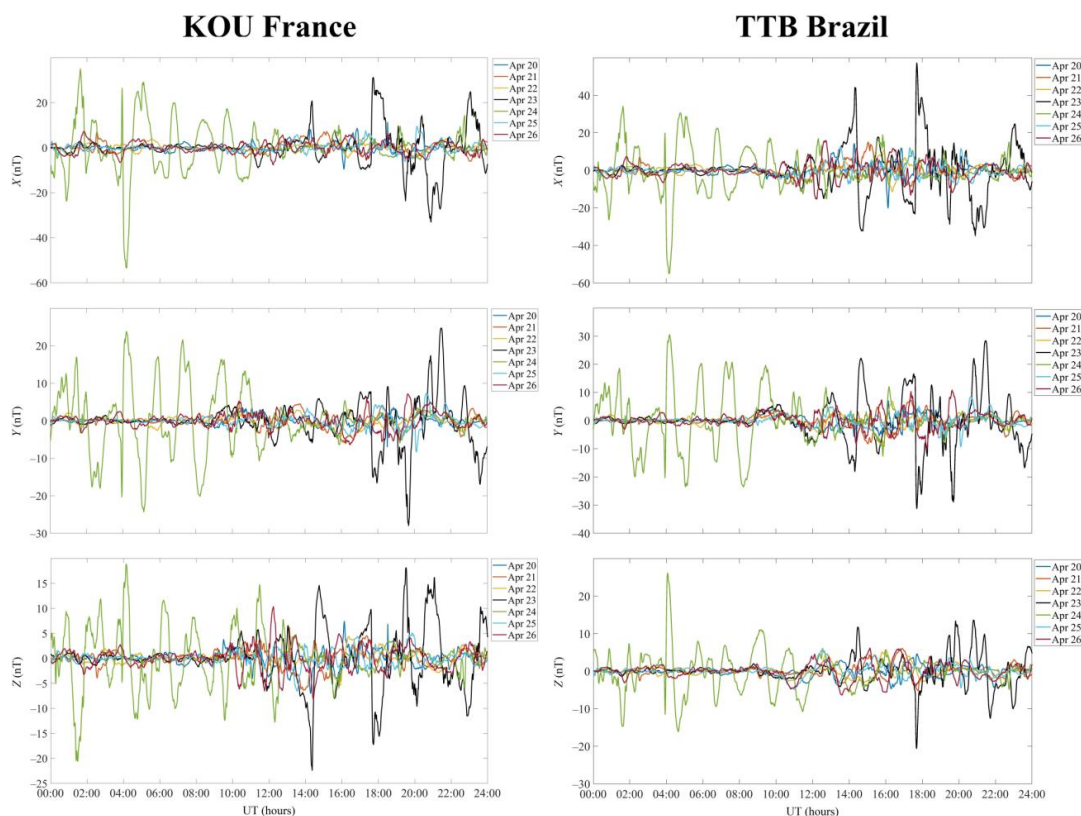
218 *KOU Station.* During magnetically quiet times, as well as until 14:00 UT on 23 April 2023, the variations in the
219 strength of the northward component of the geomagnetic field, X , were smaller than ± 10 nT (Fig. 5). Over the period
220 11:00 UT on 23 April 2023 to 16:00 UT on 24 April 2023, the X -component showed significant enhancements in its
221 variations that become non-monotonous, with a maximum of 35 nT at 21:00 UT on 23 April 2023 and a minimum
222 of -53 nT at 04:10 UT on 24 April 2023.

223
224
225
226
227
228

During the quiet time reference period, the eastward component of the geomagnetic field, Y , exhibited variations
attaining ± 8 nT, whereas its strength considerably decreased, to -27 nT, at 19:40 UT on 23 April 2023, after which
it increased to 52 nT at 21:30 UT. Between 00:00 UT and 12:00 UT on 24 April 2023, the Y -component showed
large non-monotonous fluctuations in strength attaining ± 25 nT.

229
230
231
232
233
234

The vertical component of the geomagnetic field, Z , showed strength fluctuations usually smaller than $\pm(5-7)$ nT,
while significant time variations in strength persisted for the period 10:00 UT on 23 April to 16:00 UT on 24 April
2023, with a minimum of about -22.5 nT at around 14:20 UT on 23 April 2023 and a maximum of ~ 18 nT at
approximately 19:30 UT on the same day. During the course of the day 24 April 2023, the Z -component exhibited
variations within -21 nT to 19 nT.



235
236
237
238

Figure 5: UT variations of the geomagnetic field at the KOU station (geographic coordinates 5.2100°N, 52.730°W, geomagnetic coordinates 13.87°N, 20.46°E) and at the TTB station (geographic coordinates 1.2050°S, 48.5130°W, geomagnetic coordinates 7.25°N, 24.35°E) over the period 20–26 April 2023.

239
240
241
242
243

TTB Station. On quiet time reference days, the northward component of the geomagnetic field, X , showed variations smaller than ± 20 nT (Fig. 5), which developed into non-monotonous and significant variations over a span of time between $\sim 10:00$ UT on 23 April 2023 and $\sim 16:00$ UT on 24 April 2023. The field strength had minimums of -35 nT and -55 nT at $\sim 21:00$ UT on 23 April 2023 and at $04:10$ UT on 24 April 2023, respectively, and a maximum of 57 nT at $17:40$ UT on 23 April 2023.

244

245
246
247
248

The quiet time eastward component of the geomagnetic field, Y , strength usually exhibited variations smaller than ± 10 nT, whereas on 23 April 2023 a minimum strength of -31 nT was recorded at $\sim 17:45$ UT and a maximum of about 29 nT at $21:35$ UT on 23 April 2023. The significant variations in the Y -component persisted through to $18:00$ UT on 24 April 2023, with a maximum of 30 nT at $04:10$ UT on 24 April 2023.

249

250
251

During magnetically quiet times, the vertical component of the geomagnetic field, Z , exhibited variations within ± 7 nT. Approximately from $12:00$ UT on 23 April 2023 to $19:00$ UT on 24 April 2023, this component showed fluctuations in strength from -20 nT to 26 nT.

252

253

254
255
256
257

PIL Station. On quiet time reference days, the northward component of the geomagnetic field, X , exhibited strength variability within ± 10 nT (Fig. 6), while it showed a significant increase in non-monotonous variations over the interval $11:00$ UT on 23 April 2023 to $14:00$ UT on 24 April 2023. The positive spikes of 37 nT and 47 nT were observed to occur at $17:40$ UT on 23 April 2023 and at $\sim 04:00$ UT on 24 April 2023, respectively, while the negative spikes of -47 nT and -68 nT to occur at $21:00$ UT on 23 April 2023 and at $04:10$ UT on 24 April 2023, respectively.

258

259

260



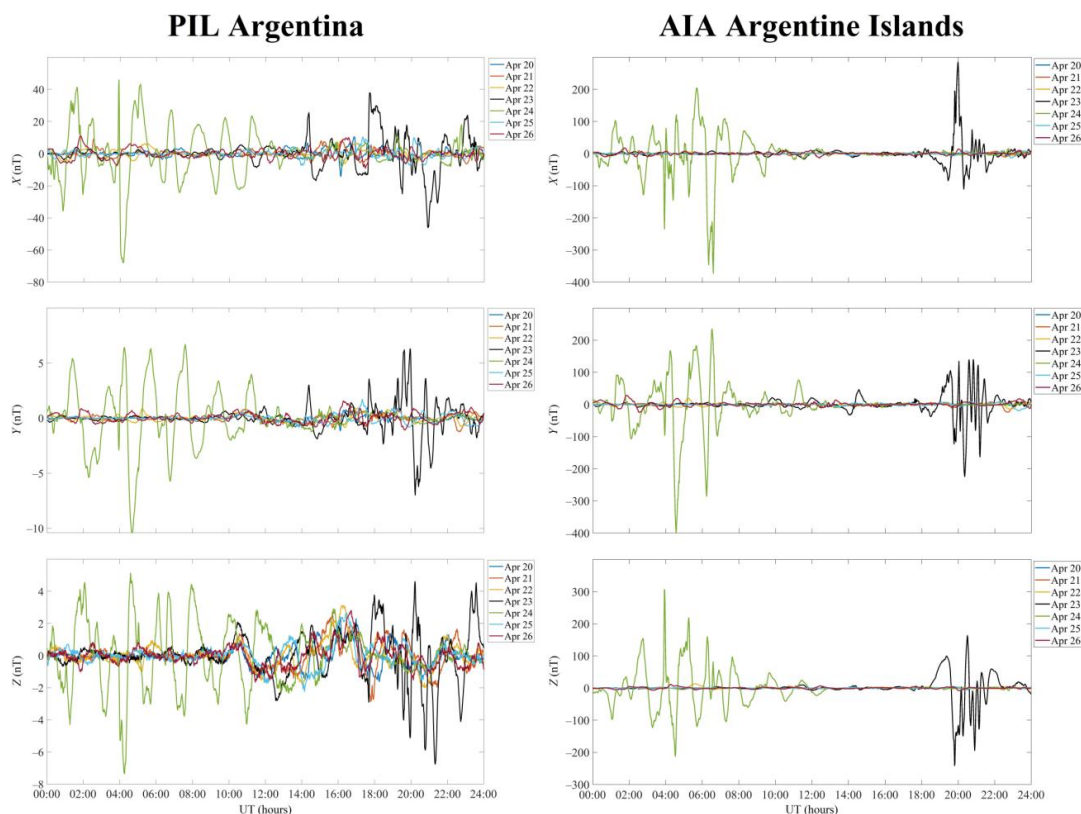
261 The eastward component of the geomagnetic field, Y , strength showed variability within a few nT under quiet time
262 conditions, while from 12:00 UT on 23 April 2023 to 16:00 UT on 24 April 2023 this component variations became
263 non-monotonous and significant, with spike strengths attaining 6.5 nT and alternating decrease strengths reaching -7
264 nT over the interval 19:00 UT to 20:00 UT on 23 April 2023, and a drop of -10.5 nT at approximately 04:40 UT on
265 24 April 2023.

266
267 During magnetically quiet times, the vertical component of the geomagnetic field, Z , showed variations smaller than
268 a few nT, whereas it exhibited considerable and sharp variations from 10:00 UT on 23 April 2023 to 16:00 UT on 24
269 April 2023. The Z -component strength fell to -7.3 nT at approximately 04:10 UT on 24 April 2023, while its
270 magnitude was close to 3 nT at about 16:00 UT.

271
272 *AIA Station.* On quiet time reference days, the northward component of the geomagnetic field, X , exhibited strengths
273 rarely exceeding ± 20 nT (Fig. 6). The considerable and sharp variations in this component strength began at around
274 18:00 UT on 23 April 2023 and continued until 12:00 UT on 24 April 2023. During 23 April 2023, the X -component
275 strength was observed to vary from -100 nT to 290 nT, while it showed greater variability on 24 April 2023 when
276 the strength varied from -380 nT to 200 nT.

277
278 The quiet time eastward component of the geomagnetic field, Y , strength showed variability within ± 30 nT. The
279 significant and sharp variations in the Y -component began at 13:00 UT on 23 April 2023 and persisted for 24 h. On
280 23 April 2023, the Y -component showed strength fluctuations from -230 nT to 150 nT, which increased from -400
281 nT to 240 nT on 24 April 2023.

282
283 Under quiet time conditions, the vertical component of the geomagnetic field, Z , exhibited fluctuations in strength
284 smaller than ± 20 nT. From 18:00 UT on 23 April 2023 to 13:00 UT on 24 April 2023, the strength variations were
285 sharp and significant. The Z -component showed strength variations within -250 – 170 nT on 23 April 2023, and
286 within -215 – 300 nT on 24 April 2023.



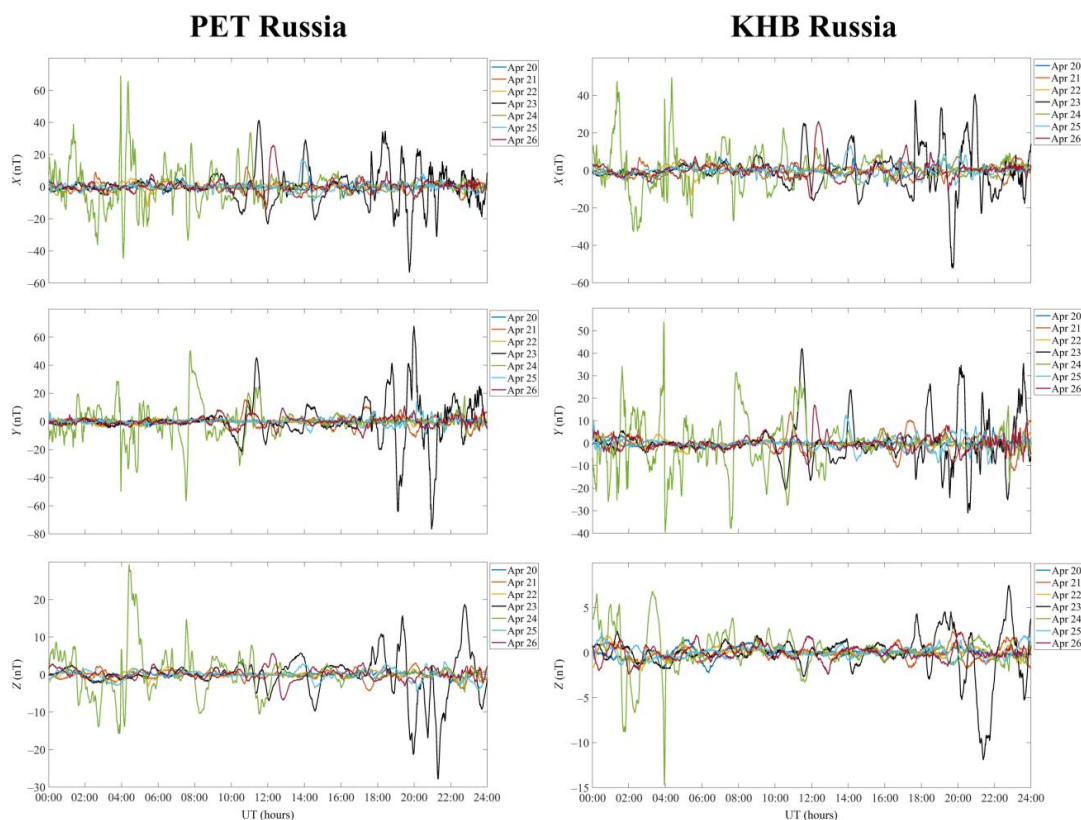
287
288 **Figure 6:** UT variations of the geomagnetic field at the PIL station (geographic coordinates 31.6670°S, 63.881°W,
289 geomagnetic coordinates 22.33°S, 8.08°E) and at the AIA station (geographic coordinates 65.2450°S, 64.2580°W,
290 geomagnetic coordinates -55.91°, +6.30°) over the period 20–26 April 2023.

291 4.2. Eastern Hemisphere

292 *PET Station.* On quiet time reference days, the northward component of the geomagnetic field, X, exhibited
293 moderate variability within ± 10 nT (Fig. 7). Considerable and sharp strength variations began after 10:30 UT on 23
294 April 2023 and persisted past 11:30 UT on 24 April 2023, with the strength fluctuating within -55 nT–43 nT on 23
295 April 2023, and from -45 nT to 70 nT on 24 April 2023.

296
297 The quiet time eastward component of the geomagnetic field, Y, strength variations were smaller than ± 15 nT. The
298 amplitude fluctuations considerably increased past 10:00 UT on 23 April 2023 and persisted until 12:00 UT on 24
299 April 2023. In the course of the first day, the amplitude fluctuations in strength occurred within -77 nT to 70 nT,
300 while they occurred around a lower strength level, from -57 nT to 50 nT, on the second day.

301
302 During the quiet time reference period, the vertical component of the geomagnetic field, Z, showed fluctuations in
303 strength with amplitudes varying from about -7 nT to 6 nT. The fluctuations notably increased after 10:00 UT on 23
304 April 2023 and continued until 13:00 UT on 24 April 2023. On 23 April 2023, the Z-component exhibited variations
305 in strength from -28 nT to 18 nT, while it showed variations from -15 nT to 29 nT the next day.



306
307 **Figure 7: UT variations of the geomagnetic field at the PET station (geographic coordinates 52.9710°N, 158.2480°E,**
308 **geomagnetic coordinates +46.63, +222.93) and at the KHB station (geographic coordinates 47.61°N, 134.68°E,**
309 **geomagnetic coordinates 39.05°N, 156.42°W) over the period 20–26 April 2023.**

310 *KHB Station.* On quiet time reference days, the northward component of the geomagnetic field, X, strength showed
311 variations generally not exceeding ± 10 nT (Fig. 7). The pronounced enhancements in sharp variations of the X-
312 component strength began after about 11:00 UT on 23 April 2023 and continued until 16:00 UT on 24 April 2023.
313 On 23 April 2023, the X-component strength exhibited variations within -50 nT to 40 nT, and it showed variations
314 from -30 nT to 50 nT on 24 April 2023.

315
316 The quiet time eastward component of the geomagnetic field, Y, variations were observed to occur mainly within
317 ± 10 nT, rarely attaining 20 nT. The amplitude fluctuations showed a noticeable increase after 10:00 UT on 23 April
318 2023, with the disturbance continuing through to 14:00 UT on 24 April 2023. On the first day, the Y-component
319 showed fluctuations from -30 nT to 43 nT, and on the second day within -39 nT to 54 nT.

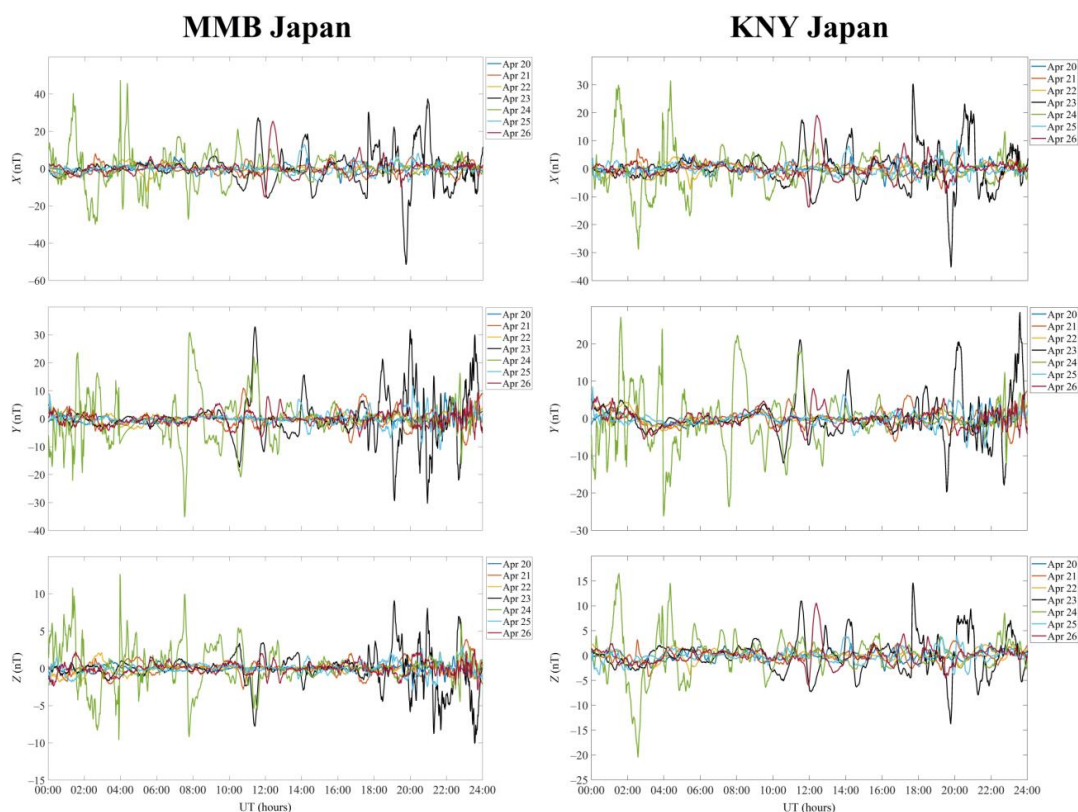
320
321 The vertical component of the geomagnetic field, Z, exhibited insignificant temporal variability within ± 2 nT on the
322 days used as a quiet time reference period, whereas the strength was observed to increase to 7.5–12 nT on 23 April
323 2023. On 24 April 2023, the component showed strength fluctuations within -14.5 nT to 7 nT. In total, the enhanced
324 fluctuations persisted for about 26 h.

325
326 *MMB Station.* The strengths of the northward component of the geomagnetic field, X, showed quiet time variations
327 generally smaller than ± 20 nT, but most frequently they were confined to ± 10 nT (Fig. 8). Enhanced variations in
328 the X-component strength began before 10:00 UT on 23 April 2023 and continued through to 12:00 UT on 24 April
329 2023, with the strength of this component changing from -50 nT to 40–47 nT.

330



331 The quiet time variations in the eastward component of the geomagnetic field, Y , strength reached ± 10 nT.
332 Significant variations in the Y -component strength began at about 10:00 UT on 23 April 2023 and continued through
333 to about 13:00 UT on 24 April 2023, with the variations in this component strength not exceeding ± 35 nT on the
334 first day, and showing temporal variability within $\pm(30\text{--}35)$ nT on the second day.
335
336 On the days used as a quiet time reference period, the vertical component of the geomagnetic field, Z , strength
337 exhibited temporal variability within a few nT, whereas they noticeably increased at $\sim 10:00$ UT on 23 April 2023
338 and persisted until 13:00 UT on 24 April 2023, with fluctuations attaining $\pm(10\text{--}12.5)$ nT.
339
340 *KNY Station.* The northward component of the geomagnetic field, X , generally exhibited variations in strength
341 smaller than ± 10 nT (Fig. 8). The strength fluctuations showed a sharp increase after 10:00 UT on 23 April 2023 and
342 continued to 16:00 UT on 24 April 2023. On 23 April 2023, the strength exhibited variations within -35 nT to 31
343 nT, and within -28 nT to 32 nT the following day.
344
345 The quiet time variations in the eastward component of the geomagnetic field, Y , strength occurred within ± 8 nT.
346 After 10:30 UT on 23 April 2023, the strength fluctuations increased from -12 nT to 28 nT. The next day, this
347 component strength exhibited temporal variability within -26 nT to 27 nT.
348
349 On the quiet time reference days, the vertical component of the geomagnetic field, Z , showed variations in strength
350 from -6 nT to 11 nT. The strength variations exhibited a noticeable increase after 10:00 UT on 23 April 2023 and
351 continued through to about 16:00 UT on 24 April 2023, with the fluctuations within ± 20 nT.
352
353 *GUA Station.* The quiet time variations in the northward component of the geomagnetic field, X , generally did not
354 exceed $7\text{--}8$ nT (Fig. 9). Enhanced strength fluctuations were observed to occur over the interval 10:00 UT on 23
355 April 2023 to 06:00 UT on 24 April 2023. On 23 and 24 April 2023, the strength of this component varied from -30
356 nT to 47 nT, occasionally to 70 nT.
357



358
359
360
361

Figure 8: UT variations of the geomagnetic field at the MMB station (geographic coordinates 43.91°N, 144.19°E, geomagnetic coordinates 36.09°N, 147.57°W) and at the KNY station (geographic coordinates 31.42°N, 130.88°E, geomagnetic coordinates 22.70°N, 158.28°W) over the period 20–26 April 2023.

362
363
364
365
366
367

The eastward component of the geomagnetic field, Y , exhibited fluctuations in strength within ± 5 nT on the days used as a quiet time reference period. Enhancements in the strength fluctuations occurred over the interval 10:00 UT on 23 April 2023 to 14:00 UT on 24 April 2023. On the first day, the strength of this component varied from -8 nT to 12 nT, and on the second day it varied within -12 nT to 13 nT. A brief ~ 19 -nT drop in the strength of this component was seen at around 04:00 UT on 24 April 2023.

368
369
370
371
372
373

The vertical component generally exhibited variations in the strength smaller than a few nT. Noticeable increases in the variations of the strength of this component were observed to occur over the interval 10:00 UT on 23 April 2023 to 05:00 UT on 24 April 2023. On 23 April 2023, the Z -component strength fluctuations occurred within ± 7 nT, while the following day they exhibited variations within -10 nT to 12 nT, with a brief decrease by 23 nT at about 04:00 UT.

374
375
376
377
378

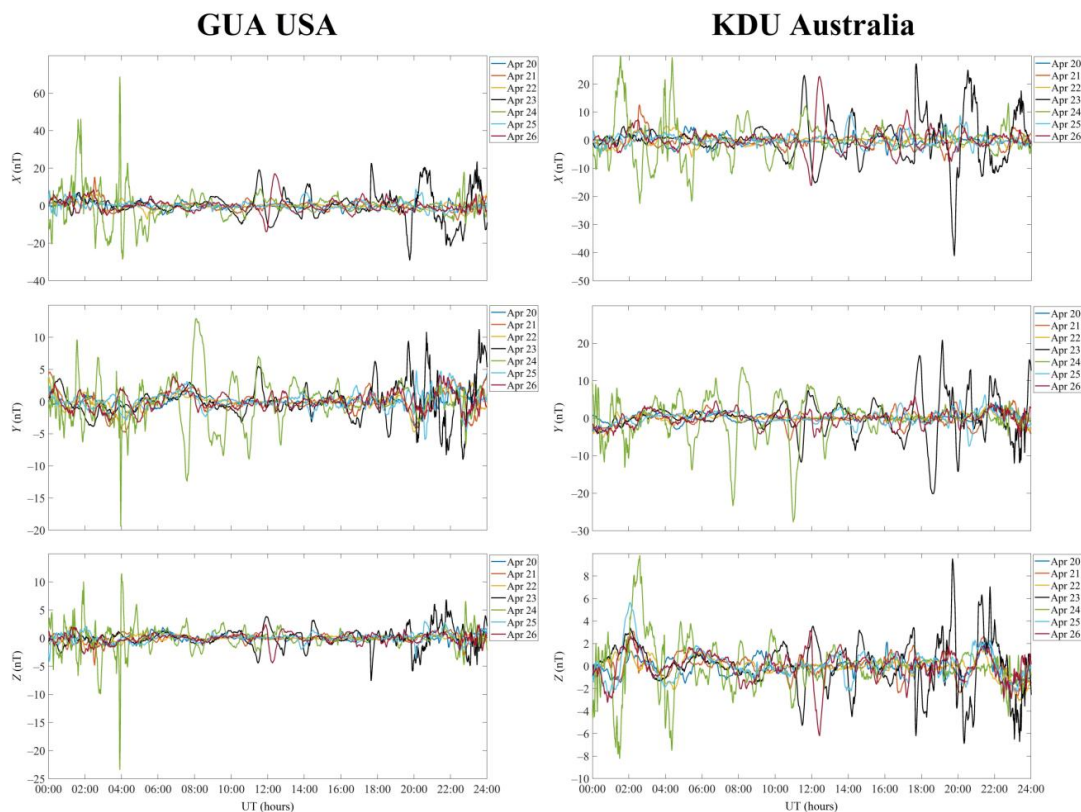
KDU Station. On the days used as a quiet time reference period, the variations in the strength of the northward component of the geomagnetic field, X , were observed to occur within ± 6 nT (Fig. 9). On 23 April 2023, the fluctuations in strength occurred within -42 nT to 28 nT from 10:00 UT to 24:00 UT. From 00:00 UT to 12:00 UT the next day, the X -component exhibited variations within -23 nT to 30 nT.

379
380
381
382
383

The eastward component of the geomagnetic field, Y , strength was observed to fluctuate within about -7 nT to 6 nT on the quiet days. From 10:00 UT to 24:00 UT on 23 April 2023, the level of strength fluctuations enhanced to ± 20 nT. The following day, the Y -component strength showed variations within -27 nT to 15 nT over the interval 00:00 UT to 13:00 UT.



384 Generally, the vertical component of the geomagnetic field, Z , showed variations in strength smaller than ± 3 nT.
385 Over the interval 10:00 UT on 23 April 2023 to 05:00 UT on 24 April 2023, a noticeable increase in the level of
386 strength fluctuations was recorded, down to -8 nT and up to ~ 10 nT.
387



388
389 **Figure 9:** UT variations of the geomagnetic field at the GUA station (geographic coordinates 13.59°N, 144.87°E,
390 geomagnetic coordinates 6.10°N, 143.44°W) and at the KDU station (geographic coordinates 12.69°S, 132.47°E,
391 geomagnetic coordinates 20.96°S, 153.66°W) over the period 20–26 April 2023.

392 *ASP Station.* The northward component of the geomagnetic field, X , showed the quiet time variability of strength
393 mainly within $\pm(3-10)$ nT (Fig. 10). The enhancement in strength fluctuations with peak-to-peak amplitude of -53
394 nT to 32 nT was observed to occur between 10:00–24:00 UT on 23 April 2023, while between 00:00–06:00 UT the
395 next day, the X -component strength exhibited temporal variability within -28 nT to 39 nT.
396

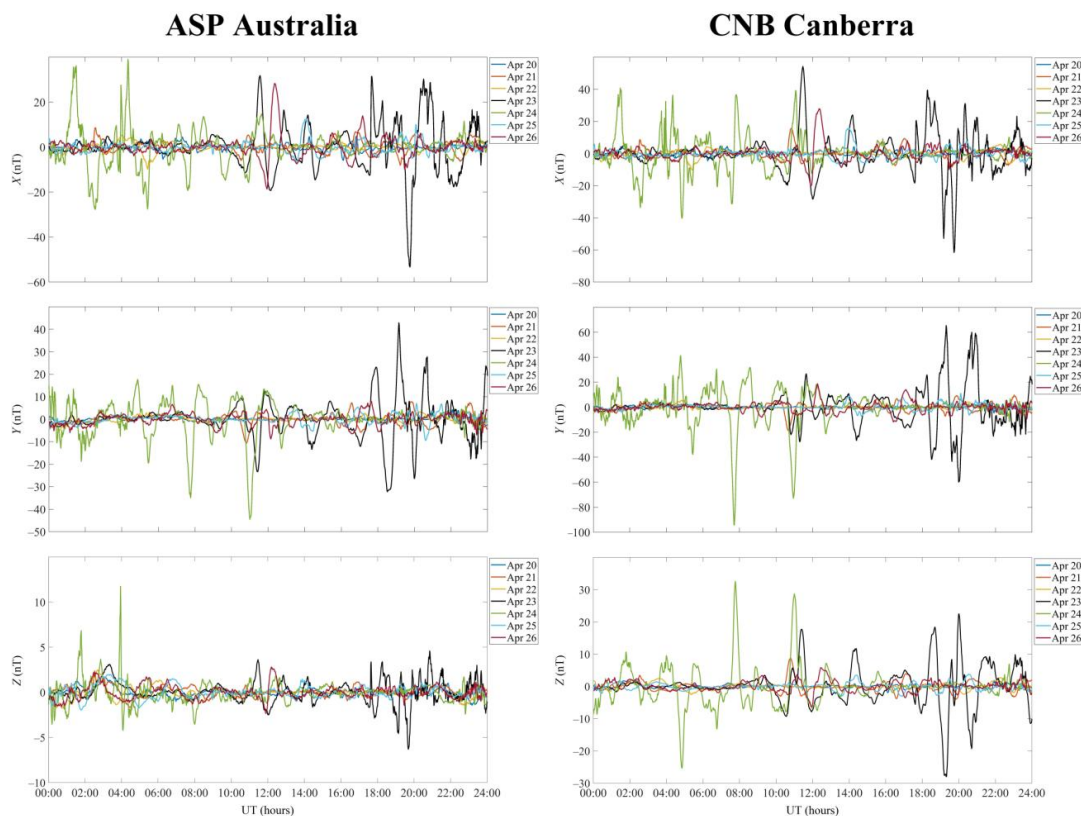
397 During quiet days, the eastward component of the geomagnetic field, Y , exhibited strength variations smaller than
398 ± 10 nT, which then significantly enhanced beginning at about 10:00 UT on 23 April 2023 and persisted until 13:00
399 UT on 24 April 2023. On the first day, the level of strength fluctuations was found between -33 nT and 43 nT, while
400 on the second day it varied from -44 nT to 15 nT.
401

402 On the days used as a quiet time reference period, the vertical component of the geomagnetic field, Z , exhibited
403 temporal variability within ± 3 nT. From 10:00 UT to 24:00 UT on 23 April 2023, the Z -component showed an
404 increase in strength fluctuations from -6.5 nT to 5 nT, while on the following day it exhibited fluctuations from -5
405 nT to 12 nT.
406

407 *CNB Station.* On the quiet days, the northward component of the geomagnetic field, X , showed variations in strength
408 mainly from -10 nT to 10 nT (Fig. 10). Significant enhancements in strength began at around 10:00 UT on 23 April



409 2023 and continued through to 12:00 UT on 24 April 2023. The strength of this component was observed to vary
410 from -62 nT to 55 nT on the first day, and within ± 40 nT from 00:00 UT to 12:00 UT on the second day.
411



412
413 **Figure 10:** UT variations of the geomagnetic field at the ASP station (geographic coordinates 23.76°S , 133.88°E ,
414 geomagnetic coordinates 31.83°S , 151.20°W) and at the CNB station (geographic coordinates 35.32°S , 149.36°E ,
415 geomagnetic coordinates 41.75°S , 132.81°W) over the period 20–26 April 2023.

416 On the days used as a quiet time reference period, the eastward component of the geomagnetic field, Y, showed
417 strength fluctuations not exceeding ± 20 nT. Between 10:00 UT and 24:00 UT on 23 April 2023, the Y-component
418 exhibited variations in strength from -60 nT to 64 nT, and during the interval 00:00 UT to 12:00 UT on 24 April
419 2023, from -95 nT to 43 nT.

420
421 The vertical component of the geomagnetic field, Z, showed quiet time variations in strength smaller than ± 8 nT.
422 Considerable enhancements in sharp variations in the strength of this component began at about 10:00 UT on 23
423 April 2023 and persisted until 12:00 UT on 24 April 2023, with the Z-component strength varying from -28 nT to
424 33 nT.

425
426 *MCQ Station.* On the quiet days, the northward component of the geomagnetic field, X, was observed to vary from $-$
427 40 nT to 70 nT (Fig. 11), with the exception of a decrease by 380 nT and an increase by 200 nT in strength at around
428 12:00 UT on 26 April 2023, as well as decreases by 160 nT and 120 nT at around 11:00 UT and 14:00 UT on 21 and
429 25 April 2023, respectively. Significant and sharp increases in amplitude and frequency fluctuations began at 10:00
430 UT on 23 April 2023 and stopped at around 12:00 UT on 24 April 2023, with the strength fluctuating within -530
431 nT to 470 nT.
432



433 On the days used as a quiet time reference period, the eastward component of the geomagnetic field, Y , showed
434 variations in strength smaller than 30–40 nT, with the exception of a drop of about 200 nT that followed an increase
435 by 100 nT near 12:00 UT on 26 April 2023. A significant rise in amplitude and frequency fluctuations was observed
436 to occur after 10:00 UT on 23 April 2023 and continued until 12:00 UT on 24 April 2023, when the Y -component
437 strength varied from –600 nT to 340 nT.

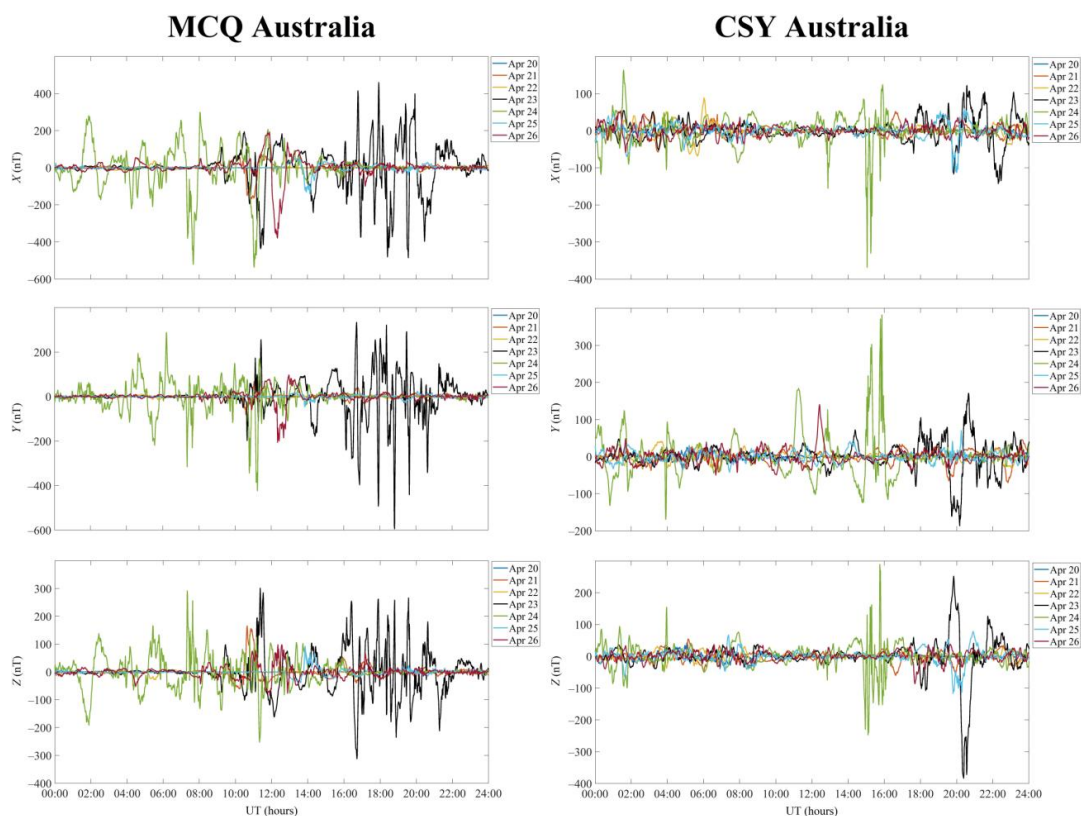
438
439 Over the intervals 12:00–14:30 UT on 25 and 26 April 2023, the vertical component of the geomagnetic field, Z ,
440 strength exhibited variability within –80 nT to 100 nT. On 21 April 2023, the strength reached 160 nT. In the course
441 of all other quiet days, this component showed variations not exceeding a few tens of nT. From 10:00 UT on 23
442 April 2023 to 12:00 UT on 24 April, the Z -component exhibited a sharp increase in temporal variability and the
443 level of strength fluctuations. The strength variations reached ± 320 nT.

444
445 *CSY Station.* The northward component of the geomagnetic field, X , exhibited strength fluctuations generally
446 smaller than ± 50 nT on the days used as a quiet time reference period (Fig. 11). Sporadically, they reached ± 100 nT.
447 Significant variations began after 17:00 UT on 23 April 2023 and persisted for about 24 h. On 23 April 2023, the
448 strength of this component showed a decrease to –150 nT and increases to 100–110 nT. In the 24 April 2023
449 morning, the strength of this component showed variations within –100 nT to 160 nT. On the days used as a quiet
450 time reference period, the eastward component of the geomagnetic field, Y , showed variations usually not exceeding
451 $\pm(30\text{--}40)$ nT, whereas the strength fluctuations reached ± 180 nT during the storm.

452
453 The vertical component of the geomagnetic field, Z , seldom exhibited variations in excess of 50 nT, with the greatest
454 variations (–380 nT to 260 nT) seen on 23 April 2023.

455
456 The particular attention should be given to significant, up to 300–380 nT, variations that were recorded in all
457 components from 12:40 UT to 16:00 UT on 24 April 2023. During this UT interval, the X -, Y -, and Z -components
458 exhibited strength fluctuations within –380–120 nT, –130–380 nT, and –250–290 nT, respectively.

459



460
461
462
463

Figure 11: UT variations of the geomagnetic field at the MCQ station (geographic coordinates 54.5°S, 158.95°E, geomagnetic coordinates 59.32°S, 116.38°W) and at the CSY station (geographic coordinates 66.283S, 110.5330E, geomagnetic coordinates -75.53°S, -174.80°W).

464 5 Discussion

465 All geomagnetic field components were a maximum during two time intervals, one from approximately 12:00 UT to
466 21:00 UT on 23 April 2023 and the other from 01:00 UT to 05:00 UT on 24 April 2023. Thus, this was a two-step
467 severe geomagnetic storm in solar cycle 25 (Ghag et al., 2024), with the K_p indices of 8.3 and 7.7, and the D_{st} index
468 equal to -170 nT and -212 nT, which is the first characteristic feature of the storm.

469 Substituting the solar wind dynamic pressure of 11 nPa and 10 nPa recorded for these two storms (Fig. 2) into the
470 expression for the energy of the magnetic storm (Gonzalez et al., 1994) yields 8.1 PJ and 9.7 PJ, with the power of
471 these storms of 173 GW and 674 GW, respectively. According to NOAA (<https://www.swpc.noaa.gov>), these
472 storms are classified as G4 (severe) geomagnetic storms. This is the second characteristic feature of the storm.

473
474
475 In the western hemisphere, the geomagnetic storm started by day on 23 April 2023, continued through the 23/24
476 April 2023 night, and ceased in the daytime on 24 April 2023. In the eastern hemisphere, the storm appeared during
477 local nighttime on 23/24 April 2023 and continued by day and at night on 24 April 2023.

478
479 Next consider the latitudinal dependence of the geomagnetic perturbations that occurred in the course of the storm.
480 The latitudinal distribution of perturbations in the strength of all geomagnetic field components on the disturbed
481 days and the days used as a quiet time reference period for the western and eastern hemispheres is presented in
482 Tables 3 and 4



483
 484
 485

Table 3 Peak-to-peak amplitude of the strength fluctuations in the geomagnetic field components recorded at the stations in the western hemisphere.

Station	Background values (nT)			Disturbed values (nT)		
	X-component	Y-component	Z-component	X-component	Y-component	Z-component
GDH	-50	-100	-100	-550	-300	-430
	+50	+100	+100	+240	+340	+390
OTT	-20	-30	-10	-710	-125	-560
	+20	+30	+10	+420	+257	+490
FRD	-15	-20	-5	-76	-70	-39
	+15	+20	+5	+67	+115	+44
SJG	-7	-7	-3	-42	-35	-11.5
	+7	+7	+3	+30	+26	+11.5
KOU	-10	-8	-7	-53	-27	-22.5
	+10	+8	+7	+35	+25	+18
TTB	-15	-10	-7	-55	-31	-20
	+15	+10	+7	+57	+29	+26
PIL	-10	-2	-2	-68	-10.5	-7.3
	+10	+2	+2	+47	+6.5	+5
AIA	-20	-30	-20	-380	-400	-250
	+20	+30	+20	+290	+240	+300

486

487 Table 3 shows that the geomagnetic field components usually exhibited variations smaller than 40–50 nT on the
 488 days used as a quiet time reference period. In the course of the severe geomagnetic storm, the geomagnetic field
 489 strength was observed to increase by a factor of 2–10, attaining 100–200 nT at low-latitude stations and 300–700 nT
 490 at high-latitude stations. Table 4 shows that the middle and low latitude stations in the eastern hemisphere recorded
 491 geomagnetic field fluctuations generally not exceeding 10–20 nT on the quiet days, whereas the storm time
 492 fluctuations exhibited an increase by a factor of 2–5, attaining 70–80 nT; however, at high latitude stations, the
 493 fluctuations were close to 500–600 nT. As expected, the magnitude of variations in the geomagnetic field increased
 494 with latitude, the variations in the strength of all component recorded at the stations nearly-equidistant from the
 495 equator were close in value, and the geomagnetic field perturbations were also close in value at close latitudes in the
 496 western and eastern hemispheres.
 497

Table 4 Peak-to-peak amplitude of the strength fluctuations in the geomagnetic field components recorded at the stations in the eastern hemisphere.

Station	Background values (nT)			Disturbed values (nT)		
	X-component	Y-component	Z-component	X-component	Y-component	Z-component
PET	-10	-10	-4	-55	-77	-28
	+10	+10	+4	+70	+70	+29
KHB	-10	-10	-2	-50	-39	-14.5
	+10	+10	+2	+50	+54	+7.5
MMB	-10	-10	-2	-50	-35	-10
	+10	+10	+2	+47	+35	+12.5
KNY	-10	-8	-4	-35	-26	-20
	+10	+8	+4	+32	+28	+17
GUA	-8	-5	-2	-30	-19	-23
	+8	+5	+2	+70	+13	+12
KDU	-6	-7	-3	-42	-27	-8
	+6	+6	+3	+30	+21	+10
ASP	-10	-10	-2	-53	-44	-6.5
	+10	+8	+3	+39	+43	+12
CNB	-10	-10	-7	-62	-95	-28
	+10	+10	+8	+55	+64	+33



MCQ	-40	-40	-50	-530	-600	-320
	+70	+40	+50	+470	+340	+300
CSY	+50	+40	-50	-380	-180	-380
	-50	-40	+50	+160	+380	+290

500

501

502

503

504

505

The northward component of the geomagnetic field, X , usually showed the greatest perturbations in strength in both hemispheres. The total durations of the disturbances were observed to be 26–30 hours. Thus, the geomagnetic storm, the strongest in solar cycle 25, being a part of the geospace storm, established the state of space weather on a global scale over 23–24 April 2023.

506

507

508

509

510

Geomagnetic field variations are produced by changing electric currents. Currents relevant to geomagnetic storms comprise the magnetopause electric current flowing eastward near the equatorial plane, the westward current through the magnetospheric tail and equatorial ring current within 3–6 earth radius from the Earth, and the ionospheric currents in high latitude ionosphere.

511

512

513

514

515

516

517

518

During substorms, the electric current in the near tail can partially be diverted into the polar ionosphere along the geomagnetic field lines closing the electric current through the substorm current wedge. As a result, the westward equatorial electric current diminishes, which should be manifested by an increase in the horizontal component of the geomagnetic field at the equator, and the westward ionospheric current increases at high latitudes, which is observed as an increase in the horizontal intensity, H , of the geomagnetic field. The magnetic effect on the surface of the Earth from the ionospheric currents significantly surpasses that from the tail current due to the proximity of the ionosphere to the ground magnetometer stations.

519

520

521

522

523

524

525

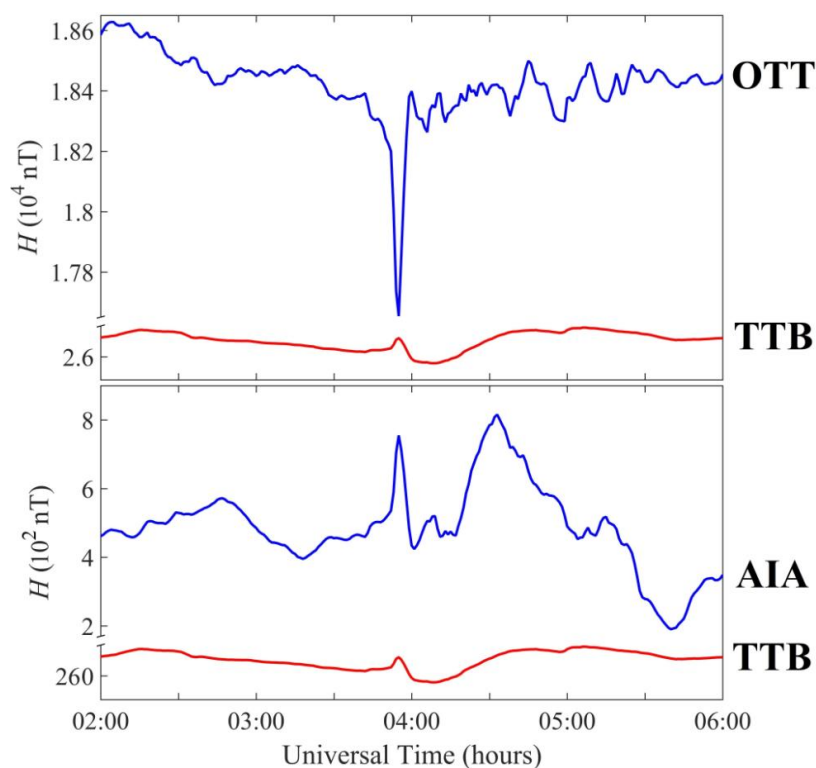
526

527

528

529

As it happened, in the observations discussed in this paper, one of the two magnetometer chain was situated in the night hemisphere of the Earth during both of the two steps of the 23–24 April 2023 geomagnetic storm. However, the anticipated manifestations of the substorm current wedge can be easily seen only during the second step of the 23–24 April 2023 geomagnetic storm along the western hemisphere chain of magnetometer stations where the storm was observed during night. The H components acquired at the equatorial latitude station TTB (geomagnetic latitude 7.15°N) and the high geomagnetic latitude OTT (geomagnetic latitude 54.28°N) station are shown in the top panel of Fig. 12. Just before 04:00 UTC, a partial diversion of the ring or tail current into the ionosphere through field-aligned currents occurred and yielded an increase in the intensity of the horizontal intensity, H , of the geomagnetic field at the TTB station and a simultaneous decrease in H at high latitude OTT station. In the southern hemisphere, the northern component is also positive (Kepko et al., 2015), as can be seen in the magnetogram acquired at AIA station (Fig. 12, bottom panel).



530
531 **Figure 12: Magnetograms from high latitude OTT and AIA stations and equatorial TTB station on the night side during**
532 **the second step of the 23–24 April 2023 geomagnetic storm.**

533 Processes analogous to those reported above are not observed during the first step of the 23–24 April 2023
534 geomagnetic storm along the eastern hemisphere chain of magnetometer stations where the first step of the storm
535 was observed during night. As was described in the Introduction section, the strength of the interplanetary magnetic
536 field B_z component attained ~ -22 nT during the first step and ~ -30 nT during the second step of the severe
537 geomagnetic storm. These observations suggest that there is a B_z threshold for diverting the cross-tail current
538 through the wedge into the ionosphere, the value of which lies between -22 nT and -30 nT for the 23–24 April 2023
539 geomagnetic storm.

540 **6 Conclusions**

541 The intercomparisons of the geomagnetic field variations recorded at two near meridional chains of magnetometer
542 stations in the western and eastern hemispheres yield the following results:

- 543 1. Part of the near-Earth cross-tail current closed itself via the ionosphere, to which it was linked by the substorm
544 current wedge, and manifested itself in the magnetograms acquired at equatorial and high latitude stations on the
545 night side of the Earth.
- 546 2. The observations suggest that the B_z interplanetary magnetic field component threshold for the formation of
547 substorm current wedge lies in the $-(22-30)$ nT interval.
- 548 3. Under quiet conditions, the geomagnetic field components usually exhibited variations not exceeding 40–50 nT in
549 the western hemisphere and 10–20 nT in the eastern hemisphere.

550
551
552
553



- 554 4. During the severe geomagnetic disturbance of 23–24 April 2023, the strength fluctuations increased by a factor of
555 2–10 and 2–5 in the western and eastern hemispheres, respectively, attaining 300–700 nT.
556
- 557 5. The northward component of the geomagnetic field, X , was observed to be most disturbed in the western and
558 eastern hemispheres. The total durations of the disturbances were observed to be 26–30 hours.
559
- 560 6. The geomagnetic field components showed variations in the strength increasing with latitude. The strength
561 fluctuations recorded at the stations nearly-equidistant from the equator were close in value. This is true for both the
562 western and eastern hemispheres.
563
- 564 7. Also close in value were the perturbations in the strength recorded at the stations at close latitudes but in different
565 hemispheres.
566
- 567 8. The first two-step severe geomagnetic storm in solar cycle 25, as a component of the geospace storm,
568 significantly affected the state of space weather on a global scale on 23–24 April 2023.

569 **Data Availability Statement**

570 The data sets discussed in this paper are freely accessible on the internet at [https://imag-](https://imag-data.bgs.ac.uk/GIN_V1/GINForms2)
571 [data.bgs.ac.uk/GIN_V1/GINForms2](https://imag-data.bgs.ac.uk/GIN_V1/GINForms2).

572 **Author contributions**

573 **LC** processed the data observed, interpreted the physics of the observations and wrote the entire manuscript.

574 **Competing interests**

575 The contact author has declared that none of the authors has any competing interests.

576 **Acknowledgements**

577 This publication makes use of data collected by INTERMAGFNET and published at [https://imag-](https://imag-data.bgs.ac.uk/GIN_V1/GINForms2)
578 [data.bgs.ac.uk/GIN_V1/GINForms2](https://imag-data.bgs.ac.uk/GIN_V1/GINForms2). The solar wind parameters have been retrieved from the Goddard Space Flight
579 Center Space Physics Data Facility <https://omniweb.gsfc.nasa.gov/form/dx1.html>. This research also draws upon
580 data provided by the World Data Center for Geomagnetism, Kyoto (data are retrieved from [http://wdc.kugi.kyoto-](http://wdc.kugi.kyoto-u.ac.jp)
581 [u.ac.jp](http://wdc.kugi.kyoto-u.ac.jp)). Special thanks are due to V. T. Rozumenko at V. N. Karazin Kharkiv National University who provided
582 useful comments on the contents of this paper. The author is grateful to his students M. B. Shevelev and Y. H.
583 Zhdanko for their assistance in preparing this paper.

584 **Financial support**

585 Support for L. F. Chernogor was also provided by Ukraine state research projects #0121U109881 and
586 #0122U001476.

587 **References**

- 588 Abe, O. E., Fakomiti, M. O., Igboama, W. N., Akinola, O. O., Ogunmodimu, O., and Migoya-Orué, Y. O.:
589 Statistical analysis of the occurrence rate of geomagnetic storms during solar cycles 20–24, *Advances in Space*
590 *Research*, 71, 2240–2251, <https://doi.org/10.1016/j.asr.2022.10.033>, 2023.
591 Al Shidi, Q., Pulkkinen, T., Toth, G., Brenner, A., Zou, S., and Gjerloev, J.: A large simulation set of geomagnetic
592 storms—Can simulations predict ground magnetometer station observations of magnetic field perturbations? *Space*
593 *Weather*, 20, e2022SW003049, <https://doi.org/10.1029/2022SW003049>, 2022.



- 594 Bothmer, V., and Daglis, I.: Space Weather: Physics and Effects, New York: Springer-Verlag,
595 <https://doi.org/10.1007/978-3-540-34578-7>, 2006.
- 596 Buonsanto, M.: Ionospheric storms — A review, *Space Sci. Revs.*, 88, 563–601,
597 <https://doi.org/10.1023/A:1005107532631>, 1999.
- 598 Carlowicz, M. J., and Lopez, R. E.: Storms from the Sun, Washington, DC: Joseph Henry Press,
599 <https://doi.org/10.17226/10249>, 2002.
- 600 Ghag, K., Raghav, A., Bhaskar, A., Soni, S. L., Sathe, B., Shaikh, Z., Dhamane, O., and Tari, P.: Quasi-planar
601 ICME sheath: A cause of first two-step extreme geomagnetic storm of 25th solar cycle observed on 23 April 2023,
602 arXiv preprint arXiv:2305.05381v2 [physics.space-ph] 12 Jan 2024, <https://arxiv.org/pdf/2305.05381.pdf>, 2024.
- 603 Chernogor, L. F.: Physics of geospace storms, *Space Science and Technology*, 27, 3–77,
604 <https://doi.org/10.15407/knit2021.01.003>, 2021a.
- 605 Chernogor, L. F.: Statistical Characteristics of Geomagnetic Storms in the 24th Cycle of Solar Activity, *Kinematics
606 and Physics of Celestial Bodies*, 37, 193–199, <https://doi.org/10.3103/S0884591321040048>, 2021b.
- 607 Chernogor, L. F., and Domnin, I. F.: Physics of geospace storms, Kharkiv: V. N. Karazin Kharkiv National
608 University Publ., 2014.
- 609 Chernogor, L. F., Garmash, K. P., Guo, Q., and Zheng, Y.: Effects of the Strong Ionospheric Storm of August 26,
610 2018: Results of Multipath Radiophysical Monitoring, *Geomagnetism and Aeronomy*, 61, 73–91,
611 <https://doi.org/10.1134/S001679322006002X>, 2021.
- 612 Chernogor, L. F., Grigorenko, Ye. I., Lysenko, V. N., and Taran, V. I.: Dynamic processes in the ionosphere during
613 magnetic storms from the Kharkov incoherent scatter radar observations, *Int. J. Geomagn. Aeron.*, 7, GI3001,
614 <https://doi.org/10.1029/2005GI000125>, 2007.
- 615 Chernogor, L. F., and Shevelev, M. B.: Latitudinal dependence of quasi-periodic variations in the geomagnetic field
616 during the greatest geospace storm of September 7-9, 2017. *Space Sci. and Technol*, 26, 72–83,
617 <https://doi.org/10.15407/knit2020.02.072>, 2020.
- 618 Daglis, I. A.: Space Storms and Space Weather Hazards, New York: Springer Dordrecht,
619 <https://www.springer.com/gp/book/9781402000300>, 2001.
- 620 Danilov, A. D., and Laštovička, J.: Effects of geomagnetic storms on the ionosphere and atmosphere. *Int. J.
621 Geomag. Aeron.*, 2, 209–224, 2001.
- 622 De Abreu, A. J., Correia, E., De Jesus, R., Venkatesh, K., Macho, E. P., and Roberto, M.: Statistical analysis on the
623 ionospheric response over South American mid- and near high-latitudes during 70 intense geomagnetic storms
624 occurred in the period of two decades, *Journal of Atmospheric and Solar-Terrestrial Physics*, 245, 106060,
625 <https://doi.org/10.1016/j.jastp.2023.106060>, 2023.
- 626 Fagundes, P. R., Tsali-Brown, V. Y., Pillat, V. G., Arcanjo, M. O., Venkatesh, K., and Habarulema, J. B.:
627 Ionospheric storm due to solar Coronal mass ejection in September 2017 over the Brazilian and African longitudes,
628 *Advances in Space Research*, 71, 46–66, <https://doi.org/10.1016/j.asr.2022.07.040>, 2023.
- 629 Freeman, J. W.: Storms in Space, Cambridge: Cambridge University Press, [https://doi.org/10.1046/j.1365-
630 246X.2002.01771.x](https://doi.org/10.1046/j.1365-246X.2002.01771.x), 2001.
- 631 Fuller-Rowell, T. J., Codrescu, M. V., Roble, R. G., and Richmond, A. D.: How does the thermosphere and
632 ionosphere react to a geomagnetic storm? Magnetic storms, in: *Geoph. Monog. Series*, edited by Tsurutani B. T.,
633 Gonzalez W. D., Kamide Y., Arballo J. K., 98, 203–226, <https://doi.org/10.1029/GM098p0203>, 1997.
- 634 Gonzalez, W. D., Jozelyn, J. A., Kamide, Y., Kroehl, H. W., Rostoker, G., Tsurutani, B. T., and Vasyliunas, V. M.:
635 What is a geomagnetic storm? *J. Geophys. Res.*, 99, 5771–5792, <https://doi.org/10.1029/93JA02867>, 1994.
- 636 Hsu, C.-T., and Pedatella, N. M.: Effects of forcing uncertainties on the thermospheric and ionospheric states during
637 geomagnetic storm and quiet periods, *Space Weather*, 21, e2022SW003216,
638 <https://doi.org/10.1029/2022SW003216>, 2023.
- 639 Kamide, Y., and Maltsev, Y. P.: Geomagnetic Storms. In: Kamide Y., Chian A. Handbook of the Solar-Terrestrial
640 Environment., Berlin, Heidelberg: Springer-Verlag, 355–374, https://doi.org/10.1007/978-3-540-46315-3_14, 2007.
- 641 Katsko, S. V., Emelyanov, L. Ya., and Chernogor, L. F.: Features of the Ionospheric Storm on December 21-24,
642 2016, *Kinematics and Physics of Celestial Bodies*, 37, 85–95, <https://doi.org/10.3103/S0884591321020045>, 2021.
- 643 Kepko, L., McPherron, R.L., Amm, O., Apatenkov, S., Baumjohann, W., Birn, J., Lester, M., Nakamura, R.,
644 Pulkkinen, T.I., and Sergeev, V.: Substorm Current Wedge Revisited, *Space Sci. Rev.*, 190, 1–46,
645 <https://doi.org/10.1007/s11214-014-0124-9>, 2015.
- 646 Kleimenova, N. G., Kozyreva, O. V., Michnowski, S., and Kubicki, M.: Effect of magnetic storms in variations in
647 the atmospheric electric field at midlatitudes, *Geomagn. Aeron.*, 48, 622–630,
648 <https://doi.org/10.1134/S0016793208050071>, 2008.



- 649 Kleimenova, N.G., Kubicki, M., Odzimek, A., Malysheva, L. M., and Gromova L. I.: Effects of geomagnetic
650 disturbances in daytime variations of the atmospheric electric field in polar regions, *Geomagn. Aeron.* 57, 266–273,
651 <https://doi.org/10.1134/S0016793217030070>, 2017.
- 652 Koskinen, H. E. J.: *Physics of space storms. From Solar Surface to the Earth*, Berlin, Heidelberg: Springer-Verlag,
653 <https://doi.org/10.1007/978-3-642-00319-6>, 2011.
- 654 Laskar, F. I., Sutton, E. K., Lin, D., Greer, K. R., Aryal, S., and Cai, X.: Thermospheric temperature and density
655 variability during 3-4 February 2022 minor geomagnetic storm, *Space Weather*, 21, e2022SW003349,
656 <https://doi.org/10.1029/2022SW003349>, 2023.
- 657 Laštovička, J.: Effects of geomagnetic storms in the lower ionosphere, middle atmosphere and troposphere. *J.*
658 *Atmos. Terr. Phys.*, 58, 831–843, [https://doi.org/10.1016/0021-9169\(95\)00106-9](https://doi.org/10.1016/0021-9169(95)00106-9), 1996.
- 659 Lilensten, J., and Bornarel, J.: *Space Weather, Environment and Societies*, Berlin/New York: Springer,
660 <https://doi.org/10.1007/1-4020-4332-5>, 2006.
- 661 Lin, D., Wang, W., Merkin, V. G., Huang, C., Oppenheim, M., and Sorathia, K.: Origin of dawnside subauroral
662 polarization streams during major geomagnetic storms. *AGU Advances*, 3, e2022AV000708,
663 <https://doi.org/10.1029/2022AV000708>, 2022.
- 664 Luo, Y., Chernogor, L. F., Garmash, K. P., Guo, Q., Rozumenko, V. T., and Zheng, Y.: Dynamic processes in the
665 ionosphere during the 30 August–2 September 2019 geospace storm: influence on high
666 frequency radio wave characteristics, *Ann. Geophys.*, 39, 657–685, <https://doi.org/10.5194/angeo-39-657-2021>,
667 2021a.
- 668 Luo, Y., and Chernogor, L. F.: Characteristic Features of the Magnetic and Ionospheric Storms on December 21–24,
669 2016, *Kinematics and Physics of Celestial Bodies*, 38, 262–278, <https://doi.org/10.3103/S0884591322050051>, 2022.
- 670 Luo, Y., Chernogor, L. F., and Garmash, K. P.: Magneto-Ionospheric Effects of the Geospace Storm of March 21–
671 23, 2017, *Kinematics and Physics of Celestial Bodies*, 38, 210–229, <https://doi.org/10.3103/S0884591322040055>,
672 2022.
- 673 Luo, Y., Guo, Q., Zheng, Y., Garmash, K. P., Chernogor, L. F., and Shulga, S. N.: Geospace storm effects on
674 August 5–6, 2019 (in Ukrainian), *Space Science and Technology*, 27, 45–69,
675 <https://doi.org/10.15407/knit2021.02.045>, 2021b.
- 676 Moldwin, M.: *An introduction to space weather*, Cambridge: Cambridge University Press,
677 <https://doi.org/10.1017/CBO9780511801365>, 2008.
- 678 Oikonomou, C., Haralambous, H., Paul, A., Ray, S., Alfonsi, L., Cesaroni, C., and Sur, D.: Investigation of the
679 negative ionospheric response of the 8 September 2017 geomagnetic storm over the European sector, *Advances in*
680 *Space Research*, 70, 1104–1120, <https://doi.org/10.1016/j.asr.2022.05.035>, 2022.
- 681 Prölss, G. W.: Ionospheric F-region storms, in: *Handbook of Atmospheric Electrodynamics*, edited by Volland H.,
682 Florida, USA: CRC Press, Boca Raton, <https://doi.org/10.1201/9780203713297>, 2, 195–248, 1995.
- 683 Prölss, G. W., and Roemer, M.: Thermospheric storms, *Adv. Space Res.*, 7, 223–235, [https://doi.org/10.1016/0273-1177\(87\)90096-2](https://doi.org/10.1016/0273-1177(87)90096-2), 1987.
- 685 Qian, L., Wang, W., Burns, A. G., Chamberlin, P. C., Coster, A., Zhang, S.-R., and Solomon, S. C.: Solar flare and
686 geomagnetic storm effects on the thermosphere and ionosphere during 6–11 September 2017, *Journal of Geophysical*
687 *Research: Space Physics*, 124, 2298–2311, <https://doi.org/10.1029/2018JA026175>, 2019.
- 688 Song, P., Singer, H., and Siscoe, G.: *Space Weather*, Geophysical Monograph, Washington, DC: American
689 Geophysical Union, <https://doi.org/10.1002/9781118668351>, 2001.
- 690 Tariq, M. A., Yuyan, Y., Shah, M., Shah, M. A., Iqbal, T., and Liu, L.: Ionospheric-Thermospheric responses to the
691 May and September 2017 geomagnetic storms over Asian regions. *Advances in Space Research*, 70, 3731–3744,
692 <https://doi.org/10.1016/j.asr.2022.08.050>, 2022.
- 693 Wen, D., and Mei, D.: Ionospheric TEC disturbances over China during the strong geomagnetic storm in September
694 2017, *Adv. Space Res.*, 65, 2529–2539, <https://doi.org/10.1016/j.asr.2020.03.002>, 2020.